JCTC Journal of Chemical Theory and Computation

Article

pubs.acs.org/JCTC

Static and Field-Oriented Properties of Bowl-Shaped Polynuclear Aromatic Hydrocarbon Fragments

Laura Zoppi,[†] Andrea Ferretti,[‡] and Kim K. Baldridge*[,†]

[†]University of Zürich, Winterthurerstrasse 190, CH-8057 Zürich, Switzerland

[‡]Centro S3, CNR-Instituto Nanoscienze, via Campi 213/A, 41125, Modena, Italy

ABSTRACT: First principles techniques are used to investigate the structure, linear polarizability, and field-oriented property trends of the series of bowl shaped polynuclear aromatic hydrocarbon fragments, $C_{20}H_{10}$, $C_{30}H_{10}$, $C_{40}H_{10}$, and $C_{50}H_{10}$. Such structures represent a sequence of minimalistic, capped bucky tube units based on the corannulene molecule, with interesting technological promise imparted by their curvature. Specific issues associated with how the intrinsic dipole and static linear polarizability influences the orientation of these structures in the presence of an external electric field are addressed and shown to correlate well with a simple analytical model. At moderate electric fields, the induced dipoles become comparable and even larger than the intrinsic dipoles due to the large in-plane polarizabilities in these systems. This generates a nontrivial and field dependent orientation of the molecule that can be exploited, for example, to induce switching behavior within molecular nanojunctions.

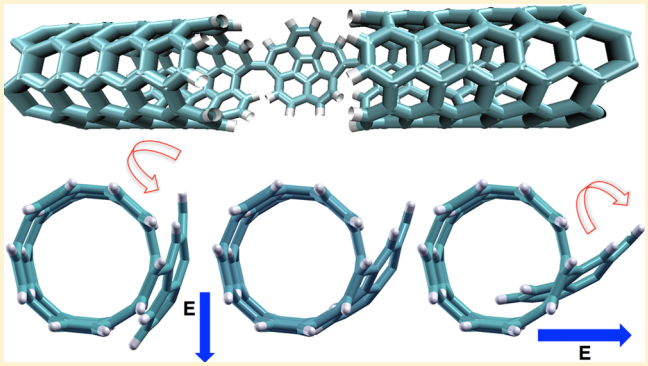

INTRODUCTION

Devices in which organic molecules constitute the active element are attracting increasing interest in the field of molecular electronics.[1] Fundamental device technology based on properties inherent in single organic molecules offers, in principle, unlimited possibilities for technological development since diverse electronic features can be tailored with adept chemical design and synthesis. The extended family of curved polynuclear aromatic hydrocarbon (PAH) fragments based on corannulene[2] offers a particularly interesting set of scaffolds for building up structures with a tunable spectrum of electronic properties. In particular, curvature is a key structural component that confines the electronic states in one or more nanoscale directions, resulting in interesting static and field-oriented materials properties.

Understanding charge transport properties of curved π-conjugated organic materials is central to their rational utilization as electrically active materials in solid state devices.[1] Studies to date have focused on intermolecular interactions of buckybowls in crystalline/dimeric systems, rather than consideration of the electrical response of individual bowls. For example, Scott and collaborators have illustrated the role of dipole−dipole and electrostatic interactions in crystalline structures in a series of curved aromatics.[3] Several other studies have analyzed curvature effects on $\pi-\pi$ stacking interactions for prototype dimeric systems.[4−6] The first and only measurement of electron transport properties of a curved aromatic bowl structure has been shown for the sumanene crystal ($C_{21}H_{12}$),[7] revealing high electron mobility along the π-bowl stacking direction and a large anisotropy, properties attributed to the curvature of the system.

Despite the great promise of π-conjugated carbon-rich systems for application in molecular electronics,[8,9] a systematic investigation of charge transport properties is still lacking. In the present work, exploration into fundamental electronic properties, such as static response functions, of a series of increasingly curved molecules based on corannulene ($C_{20}H_{10}$−$C_{50}H_{10}$) is undertaken using first principles electronic structure calculations. In particular, a detailed look at predictability and interpretation of dipole and polarizability properties is carried out as a function of theoretical methodology, and results are compared to an analytic model. The presence of strong intrinsic molecular dipoles manifested by the curvature in these structures[10] together with a large polarizable surface of π electron density are fundamental to unlocking and exploiting such systems for material devices. Moreover, structures that manifest a large intrinsic dipole can be exploited for governing molecular orientation in an electric field, which is of interest in the construction of molecular switches.[11]

THEORETICAL METHODOLOGY AND APPROACH

The structure and polarizability properties across a series of bowl-shaped polynuclear aromatic hydrocarbon (PAH) systems of increasing curvature, $C_{20}H_{10}$, $C_{30}H_{10}$, $C_{40}H_{10}$, and $C_{50}H_{10}$, have been investigated. All four systems are C_{5v} symmetric, with the 5-fold symmetry axis (z) parallel to the intrinsic molecular

Received: July 3, 2013
Published: September 10, 2013

   dx.doi.org/10.1021/ct400575p | J. Chem. Theory Comput. 2013, 9, 4797−4804

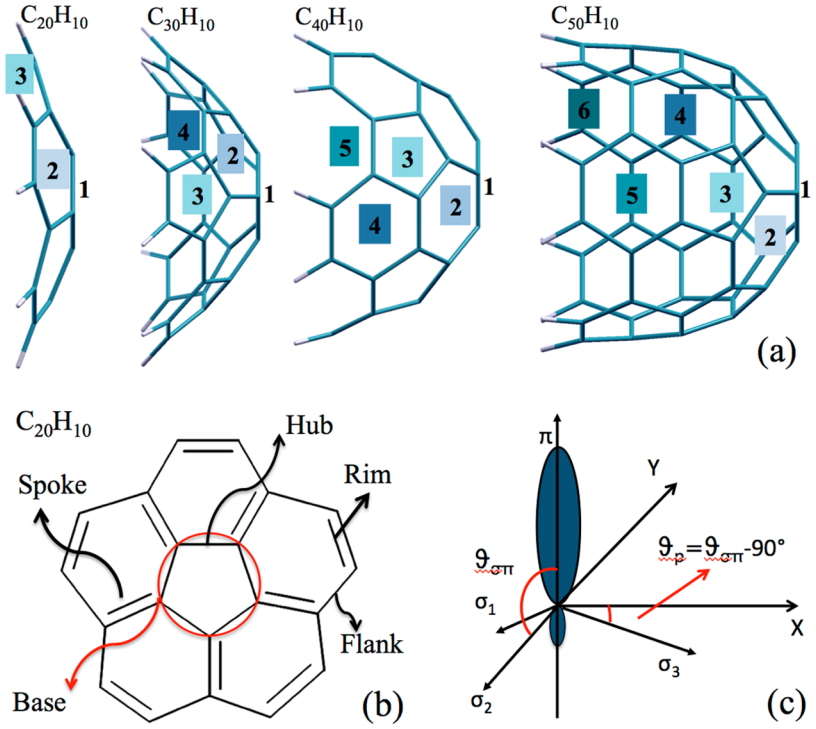

Figure 1. (a) Series of curved π $C_{20}H_{10}$–$C_{50}H_{10}$ systems with labels for rings progressing from the cap-ring (1) to the rim-ring (n). (b) Schematic representation of structural parameters of the smallest fullerene fragment, corannulene. (c) π-orbital axis vector (POAV) illustrated for a nonplanar conjugated carbon atom bonded to three atoms via schematized σ bonds, σ_1, σ_2, and σ_3; definition of the angles $\sigma\pi$ made by the π orbital to each of the σ bonds, and pyramidalization angle, $\vartheta_p = (\vartheta_{\sigma\pi} - 90°)$.

dipole. Application of an electric field polarizes the systems such that the total dipole is the sum of intrinsic and induced dipoles (P_0 and P_{ind}, respectively). In linear response theory, the induced dipole is proportional to the applied electric field, such that the total dipole can be written as

$$\mathbf{P}(\mathbf{E}) = \mathbf{P}_0 + \underline{\alpha}\mathbf{E} \tag{1}$$

where α is the static polarizability tensor. Considering the C_{5v} 5-fold rotational symmetry, the z direction is uncoupled to directions in the xy plane ($\alpha_{zx} = \alpha_{zy} = 0$). To further simplify the model, a continuous rotational symmetry (C_∞ axis) is assumed in what follows, resulting in a polarizability tensor that is approximately diagonal ($\alpha_{xx} = \alpha_{yy}$). Deviations from this oversymmetrized view were shown to be minimal in this study. Designating the polarizability components parallel and orthogonal to the intrinsic molecular dipole as $\alpha_\parallel$ and $\alpha_\perp$, respectively, the characterization of the bowl shaped fragment dipoles under the effect of an electric field requires the computation of the three scalar quantities, P_0, $\alpha_\parallel$, and $\alpha_\perp$.

By definition, the dipole and the polarizability tensor can be written as

$$\mathbf{P}(\mathbf{E}) = -\frac{\partial E_{tot}}{\partial \mathbf{E}}$$
$$\alpha_{ij} = -\frac{\partial^2 E_{tot}}{\partial E_i \partial E_j},\ \mathbf{E} = 0 \tag{2}$$

such that in linear response theory the total energy is given by

$$\Delta E_{tot}(\mathbf{E}) = E_{tot}(\mathbf{E}) - E_{tot}(\mathbf{0}) = -\mathbf{P}_0\cdot\mathbf{E} - \frac{1}{2}\mathbf{E}\underline{\alpha}\mathbf{E} \tag{3}$$

Specifically to the case of electric fields parallel and orthogonal to the intrinsic dipole, one finds

$$\Delta E_{tot}(E_\parallel) = -P_0 E_\parallel - \frac{1}{2}\alpha_\parallel |E_\parallel|^2$$
$$\Delta E_{tot}(E_\perp) = -\frac{1}{2}\alpha_\perp |E_\perp|^2 \tag{4}$$

The computation of the total dipole and the polarizability tensor can be carried out by direct evaluation of the derivatives of eq 2 at zero applied fields, or by calculating the total energy differences in the presence of (small) finite electric fields and using the results in eq 4.

Dipole moments and static polarizability tensors across the series $C_{20}H_{10}$–$C_{50}H_{10}$ were determined using first principles density functional theory (DFT).[12] Results were compared across DFT type, basis set extent, and methodology. Using the electronic structure theory approaches in the GAMESS[13] and Gaussian 09[14] software packages (for comparison), conformational analyses of all molecular systems, including structural and orbital arrangements as well as property calculations, were investigated. Full geometry optimizations at both B97D/Def2-TZVPP and B97D/Def2-TZVPPD levels of theory were carried out and uniquely characterized via second derivatives (Hessian) analysis to determine the number of imaginary frequencies and effects of zero point energy. From the fully optimized structures, calculation of polarizability was carried out with both analytic as well as numeric methods, using a broad array of functional types and basis sets, in order to investigate consistency and predictability across the set of molecules. In particular, evaluated functionals included PBE,[15] B3LYP,[16−18] M06-2X,[19,20] TPSS,[20,21] B97D,[22] and wB97XD,[23] together with an ultrafine grid specification. Evaluated basis sets include the correlation consistent basis sets of Dunning,[24] with and without augmented functions, denoted cc-pVnZ and aug-cc-pVnZ, respectively, with n = D for double, T for triple, and Q for

Table 1. Computed Topology Parameters As Indicated in Figure 1 for the B97D/Def2-TZVPP Optimized Geometries of $C_{20}H_{10}$, $C_{30}H_{10}$, $C_{40}H_{10}$, and $C_{50}H_{10}$

fragment	bowl depth (Å)	base/spoke dihedral angle	base/rim dihedral angle	$\vartheta_{\sigma\pi}$ ring 1	$\vartheta_{\sigma\pi}$ ring 2	$\vartheta_{\sigma\pi}$ ring 3	$\vartheta_{\sigma\pi}$ ring 4	$\vartheta_{\sigma\pi}$ ring 5	$\vartheta_{\sigma\pi}$ ring 6
$C_{20}H_{10}$	0.92	22.5	22.5	98.5	94.0	91.8			
$C_{30}H_{10}$	2.46	36.5	48.8	102.3	98.8	97.5	91.7		
$C_{40}H_{10}$	3.80	38.3	70.0	102.1	101.2	100.5	98.5	93.5	
$C_{50}H_{10}$	5.19	38.7	86.5	102.1	101.9	101.6	99.9	97.1	92.7

Table 2. Static Polarizability Tensors in Atomic Units, Computed Using Different Basis Sets (X) at B97D/Def2-TZVPP Optimized Geometry and Zero Field (i.e., PBE/X//B97D/Def2-TZVPP Level of Theory)

	X =						
$C_{20}H_{10}$	cc-pVDZ	aug-cc-pVDZ	cc-pVTZ	aug-cc-pVTZ	cc-pVQZ	TZVP	plane waves
xx	282.90	306.98	295.17	307.37	301.20	296.78	307
yy	282.90	306.98	295.17	307.37	301.20	296.78	307
zz	82.76	122.85	103.06	122.67	114.37	111.89	123

	X =							
$C_{20}H_{10}$	Def2-TZVP	Def2-TZVPP	Def2-TZVPD	Def2-TZVPPD	Def2-QZVP	Def2-QZVPP	Def2-QZVPD	Def2-QZVPPD
xx	299.66	300.28	306.01	306.10	304.86	304.86	306.84	306.84
yy	299.66	300.28	306.01	306.10	304.86	304.86	306.84	306.84
zz	113.85	114.40	121.55	121.64	119.72	119.72	122.28	122.28

quadruple-ζ. In addition, the more recent Def2-nZVxx sequence of basis sets is used,[25,26] with n = T for triple and n = Q for quadruple-ζ, and xx = p, pp, pd, and ppd for polarization functionality. Visualization and analysis of structural and property results were obtained using QMView[27] and WEBMO.[28]

Using the plane wave methodology in Quantum-ESPRESSO,[29] polarizabilities were first calculated for the optimized structures determined from GAMESS,[13] using fixed atomic positions, in the absence of any external electric field. The ionic contributions to dipoles and polarizabilities were investigated by performing a further relaxation of the ionic degrees of freedom in the presence of the external electric field. Due to the periodic boundary conditions in the plane-wave basis description, the finite electric field was mimicked using a sawtooth potential, linear in the space close to the molecule and with opposite slope in a limited region far from the molecule. Vanderbilt ultrasoft pseudopotentials were used with a cutoff of 30 and 250 Ry for the wave functions and the charge density, respectively. When performing geometry optimizations, the residual forces were optimized to be smaller than 10^{-4} Ry/Bohr. The computation box was taken as a 65 × 65 × 65 Bohr^3 cell. The Martyna−Tuckerman approach[30] has been adopted to deal with long-range electrostatic interactions, therefore avoiding spurious dipole−dipole contributions. Convergence with respect to size of the supercell (molecular replicas separation) was carefully checked. Results using the PBE level of theory are compared to the all-electron localized basis description of GAMESS (zero electric field).

STRUCTURAL COMPARISON

Curvature in graphite networks imparts variation in chemical properties from the flat analogues, which manifests interesting new reactivity and possibilities for creative optical and transport devices. In the series of bowl structures investigated (Figure 1a), the introduction of pentagonal geometry within the hexagonal motif causes the curving of the surface. The least curved structure in the series, corannulene, has a single five-membered ring at the base (Figure 1b), which results in a very shallow bowl structure that can interconvert between two curved bowls with an energy barrier of only 11.5 kcal/mol.[31] The remaining three structures, $C_{30}H_{10}$, $C_{40}H_{10}$, and $C_{50}H_{10}$, each have five additional five-membered rings manifesting in significantly deeper bowl geometries, 2.5 Å, 3.8 Å, and 5.2 Å, respectively (Table 1). As a result, none of these latter structures can interconvert.

Trends in bowl depth and surface curvature can be quantified using the π-orbital axis vector (POAV) method of Haddon and Scott,[32] which assigns a pyramidalization angle at each carbon. In this way, the POAV angle is defined as illustrated in Figure 1c, and the pyramidalization angle ϑp is obtained as $\vartheta p = (\vartheta\sigma_\pi - 90)°$. For reference, the $\vartheta\sigma\pi$ angle value for the highly curved C_{60} is 102° ($\vartheta p = 12°$). The angle for a cylindrical benzenoid belt is 96° ($\vartheta p = 6°$), while that for a simple flat PAH structure is ∼90° ($\vartheta p = 0°$). Unlike these references with a single POAV angle defining their structure, the capped tube structures have varying pyramidality, as defined by the progression from the cap-ring (ring 1) to the rim-ring (ring *n*). One sees from the data in Table 1 that while the smallest in the series, $C_{20}H_{10}$, has a significantly higher cap pyramidality than C_{60}, already in $C_{30}H_{10}$, the cap pyramidality is as in C_{60} and remains constant with the higher analogues. As the bowl deepens, the structure continues to show nearly constant curvature in the lower rings, and rings near the rim approach that of the cylindrical belt. The trend toward constant curvature essentially defines the transition between bowl and tube structure. This is further supported by the base/spoke angle and base/rim angle, where the former is the angle between the plane containing the base and the plane defined by the ring containing the spoke bond and the latter is defined by the base plane and the plane defined by the ring containing the topmost rim of the structure (Figure 1b). One sees in fact that the highest analogue in the series, $C_{50}H_{10}$, approaches the value expected for a tube structure, 90°.

STATIC POLARIZABILITY AND INTRINSIC MOLECULAR DIPOLE

As discussed in the previous section, one sees a systematic trend toward tube structure with increasing ring layers on the

dx.doi.org/10.1021/ct400575p | J. Chem. Theory Comput. 2013, 9, 4797−4804

curved bowl systems. It is of interest, therefore, to see if the same trends are observed in other electronic properties. Specifically, it is relevant to look at electronic polarizabilities for any relevance associated with transport properties of these systems, particularly in the deeper bowl and tube-like structural analogues. One expects a general increase in polarizability with an increase in volume of electrons, which typically occurs in the base of these bowl structures. As the bowl structure deepens (i.e., tube area increases), the volume of electrons in the base tends to increase, but also the delocalized surface area in the tube extent increases. Therefore, to fully understand the charge-carrier mobility in these structures, these properties need to be more quantitatively investigated.

A basis set investigation was first carried out for the smallest PAH system, corannulene, $C_{20}H_{10}$, in order to evaluate the effects of varying basis set for the prediction of polarizability (Table 2). As is well-known, large polarized basis sets and wave function types that include effects of correlation are required to obtain quantitative prediction of properties such as dipole and polarizability. For the series of highly symmetric bowl structures, only the diagonal components of the predicted polarizability tensors are reported since the off-diagonal contributions are zero by symmetry. Moreover, the polarizability components orthogonal to the intrinsic dipoles are found to be identical to numerical precision in all cases, due to symmetry. As illustrated in Table 2 (upper panel), predictions of polarizability show a slightly increasing trend with increasing valence extent within the correlation-consistent basis sets of Dunning, both with and without the addition of diffuse functionality. Importantly, augmentation of the basis with diffuse functionality (e.g., aug-cc-pVDZ, aug-cc-pVTZ) is found to be quite necessary to reach a consistent value. One can further consider the Def2-nZVxx sequence of basis sets (Table 2, lower panel), which perhaps shows a more convincing convergence of predicted data and the importance of diffuse functionality. In particular, prediction of polarizabilities with Def2-TZVPPD shows a well converged value that also agrees very well with the plane wave results.

Results of the basis set analysis indicated Def2-TZVPD to be optimal as the reference basis set for investigation of the effect of varying exchange and correlation function on the response properties in the corannulene molecule. The polarizability tensors calculated using several density functional treatments are shown in Table 3. The results show that semilocal and meta-GGA functionals result in larger polarizabilities (usually overestimated) than full hybrid and range-separated functionals, which are expected to provide the best accuracy. Nevertheless, variations across different functionals are found to be quite modest. In what follows, the PBE functional is adopted for all calculations, with some comparison provided using the B97D functional.

Table 3. Static Polarizability Tensors in Atomic Units, Computed Using Different Density Functionals (Y) with the Def2-TZVPD Basis Set at B97D/Def2-TZVPP Optimized Geometry and Zero Field (i.e., Y/Def2-TZVPD//B97D/Def2-TZVPP Level of Theory)

	Y =					
$C_{20}H_{10}$	PBE	B97D	B3LYP	M06-2X	TPSS	wB97xd
xx	306.01	306.11	299.04	288.87	303.63	289.91
yy	306.01	306.11	299.04	288.93	303.63	289.91
zz	121.55	121.97	121.26	119.55	120.27	120.61

Unlike flat PAH structures or closed fullerene structures, the dipole moment for curved bowl structures can be quite large. Results for intrinsic dipole and static polarizability for all B97D/Def2-TZVPP optimized PAH fragments $C_{20}H_{10}$–$C_{50}H_{10}$ are reported in Tables 4 and 5. For comparison, the experimental value for the smallest in the series, $C_{20}H_{10}$, is 2.1 D.[10] As shown in Table 4, variation in the predicted intrinsic dipole with and without the diffuse functionality or functional type (PBE vs B97D) is not significant. The same holds true when the structural optimization also includes the diffuse functionality, B97D/Def2-TZVPD level, as shown by the values in parentheses. A very good agreement with the plane-wave results is also found. Computed dipoles show a correlation with the PAH curvature (as expected), their magnitude increasing

Table 4. Comparison of Calculated Intrinsic Molecular Dipoles, in Units of Debye, at the Levels of Theory Indicated, i.e., Varying Functional Type and Basis Set[a]

	B97D		PBE		
PAH fragment	Def2-TZVPP	Def2-TZVPD	Def2-TZVPP	Def2-TZVPD	plane waves
$C_{20}H_{10}$	2.12	2.12	2.14	2.13 (2.14)	2.12
$C_{30}H_{10}$	4.42	4.45	4.48	4.49 (4.49)	4.47
$C_{40}H_{10}$	5.69	5.72	5.76	5.78 (5.78)	5.76
$C_{50}H_{10}$	6.02		6.10		6.10

[a]The geometries have optimized at zero field using B97D/Def2-TZVPP, except for the values in parentheses, where the structural optimization has been performed at the B97D/Def2-TZVPD level of theory.

Table 5. PBE/Def2-TZVPP//B97D/Def2-TZVPP and PBE/Def2-TZVPD//B97D/Def2-TZVPP Calculated Static Polarizability Tensors in Atomic Units (Bohr^3), as Compared with Plane-Wave Calculations[a]

	PBE		
PAH fragment	Def2-TZVPP	Def2-TZVPD	plane waves
	$C_{20}H_{10}$		
xx	300.28	306.01 (306.19)	307
yy	300.28	306.01 (306.19)	307
zz	114.40	121.55 (121.59)	123
	$C_{30}H_{10}$		
xx	450.15	458.87 (458.87)	461
yy	450.15	458.87 (458.87)	461
zz	211.51	219.17 (219.17)	220
	$C_{40}H_{10}$		
xx	498.89	509.40 (509.40)	511
yy	498.89	509.40 (509.40)	511
zz	350.60	357.72 (357.72)	359
	$C_{50}H_{10}$		
xx	542.43	[552.22]	555
yy	542.43	[552.22]	555
zz	496.20	[505.55]	507

[a]Values in parentheses show results of PBE/Def2-TZVPD//B97D/Def2-TZVPD for comparison. In the case of $C_{50}H_{10}$, results in square brackets have been extrapolated based on a regression between Def2-TZVPP and Def2-TZVPD data for $C_{20}H_{10}$, $C_{30}H_{10}$, and $C_{40}H_{10}$, in accord with extrapolated value = 1.0095 × value(Def2-TZVPP) + 4.6393, R^2 = 0.9999.

dx.doi.org/10.1021/ct400575p | J. Chem. Theory Comput. 2013, 9, 4797–4804

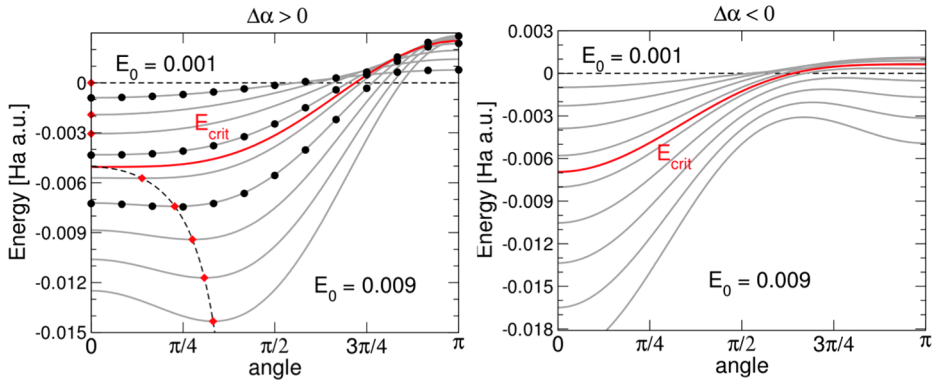

Figure 2. Model prediction for the total energy as a function of the molecule orientation with respect to external field. Left panel ($C_{20}H_{10}$ case): P_0 = 2.12 D, $\alpha_{\|}$ = 123 [Bohr^3], $\alpha_{\perp}$= 307 [Bohr^3]. Right panel: P_0 = 2.12 D, $\alpha_{\|}$ = 307 [Bohr^3], $\alpha_{\perp}$ = 123 [Bohr^3]. (Note that the right panel does not correspond to any of the systems investigated but illustrates the model prediction in the case $\Delta\alpha < 0$). Values for several field intensities are shown (ranging from 0.001 to 0.009 Ha a.u., with a step of 0.001 Ha a.u.) The curve corresponding to the critical field is highlighted in red in both panels. In the left panel, for overcritical fields the position of the energy minima is shown with red diamonds (a dashed line is added as a guide to the eye), and computed data (total energy differences) are superimposed on the plot for values of the field equal to 0.001, 0.004, and 0.006 Ha a.u.

with the molecular curvature across the series $C_{20}H_{10}$–$C_{50}H_{10}$. As with the structural properties of the series, one observes a steep rise in dipole, but a clear leveling off with a longer tube-like structure. In the lower analogues, the majority of the charge resides in the cap region that, with a deepening bowl structure, levels off due to limited additional contribution from the belt and rim rings, and the distribution in the conjugated belt area.

Results of computed static polarizability are shown in Table 5. Unlike the prediction of the dipoles, one finds a more marked dependence on the adopted basis set, as was already shown in Table 2. Again, one sees the importance of the diffuse functionality for prediction of the property (while not important for optimization of the geometry as shown in parentheses). Agreement of plane waves results with Def2-TZVPD results is found to be excellent for all the molecules. For the case of $C_{50}H_{10}$, the computational cost and numerical convergence of the calculations with the large Def2-TZVPD basis was found to be prohibitive. However, a closer analysis of the predicted $C_{20}H_{10}$–$C_{40}H_{10}$ results with and without diffuse functionality shows a strong linear correlation (extrap_val = 1.0095 × val(Def2-TZVPP) + 4.6393, R^2 = 0.9999), enabling an extrapolation of the value for $C_{50}H_{10}$. One notes a general increase in polarizability with size of the PAH system due to the effect of the diffuse functionality (e.g., ∼6, ∼8, ∼10, and ∼10 Bohr^3, with a leveling off at 10 Bohr^3).

Interestingly, across the series, one finds that the polarizability along the molecular axis (the direction of the intrinsic dipole) is smaller than those in the x and y planes, but the relative value by which it differs from the in plane polarizability indicated by the quantity $\Delta = (\alpha_{\perp} - \alpha_{\|})/\alpha_{\perp}$ decreases drastically with size of the PAH system, ∼60%, ∼50%, ∼30%, and ∼9%, respectively. In the lower analogues, with the majority of the charge in the cap region, the large polarizability in the x and y planes reflects the delocalized nature of π-electrons across this relatively large surface area, enabling the charge density to reorganize easily under the stimulus of an external electric field. Having $\alpha_{\|} < \alpha_{\perp}$ is particularly relevant because, as will be described in the next sections, dipole components along x or y may become comparable or larger than those parallel to the molecular axis when a field is applied, leading to a nontrivial response of the molecule under an external electrical stimulus. With the lengthening of the belt structure of the deeper bowls, one sees the polarizability in the z direction increasing significantly. In fact, in $C_{50}H_{10}$, polarizability along z is significantly closer to the values along the x and y directions, reflecting that increased conjugated area of the belt region, and approaching what one might find in a tube-like structure.

MOLECULAR ORIENTATION: ANALYTICAL MODEL

Following the characterization of intrinsic molecular dipole and polarizability across the series of PAH systems, it is of interest to investigate the behavior of the series (treated as linearly polarizable objects) in the presence of an electric field. This can be carried out analytically by means of a simple model, to provide expressions for the equilibrium position and stationary conditions under the appropriate molecular symmetry. The parameters of the model include strength of the field **E** (assumed with fixed orientation) and the molecular descriptors (P_0, $\alpha_{\|}$, $\alpha_{\perp}$). The molecule is treated as a rigid polarizable object with a single degree of freedom, the angle ϑ between the intrinsic dipole and the external electric field.

The total energy gain due to the presence of the field is written as

$$\Delta E_{tot} = -E_0\left[P_0 \cos\vartheta + \frac{1}{2}\alpha_{\perp}E_0 - \frac{1}{2}\Delta\alpha E_0 \cos^2\vartheta\right] \quad (5)$$

where E_0 is the intensity of the applied field and $\Delta\alpha = \alpha_{\perp} - \alpha_{\|}$. The first term in eq 5 is the energy contribution of the intrinsic molecular dipole. The remaining two terms are dependent on the molecular polarizability and describe the contribution of induced dipoles. A search for the maxima and minima of the energy as a function of the ϑ angle always results in solutions at $\vartheta_0 = 0$ and $\vartheta_1 = \pi$, corresponding to the field oriented parallel or antiparallel to the intrinsic dipole, respectively. For field intensities smaller than a defined critical value E_{crit},

$$E_{crit} = \frac{P_0}{|\alpha_{\perp} - \alpha_{\|}|} \quad (6)$$

$\vartheta_0 = 0$ always corresponds to a stable stationary point (minimum) and $\vartheta_1 = \pi$ to an unstable stationary point (maximum). For fields larger than the critical value defined in eq 6 (overcritical), a new stationary point occurs at

dx.doi.org/10.1021/ct400575p | J. Chem. Theory Comput. 2013, 9, 4797−4804

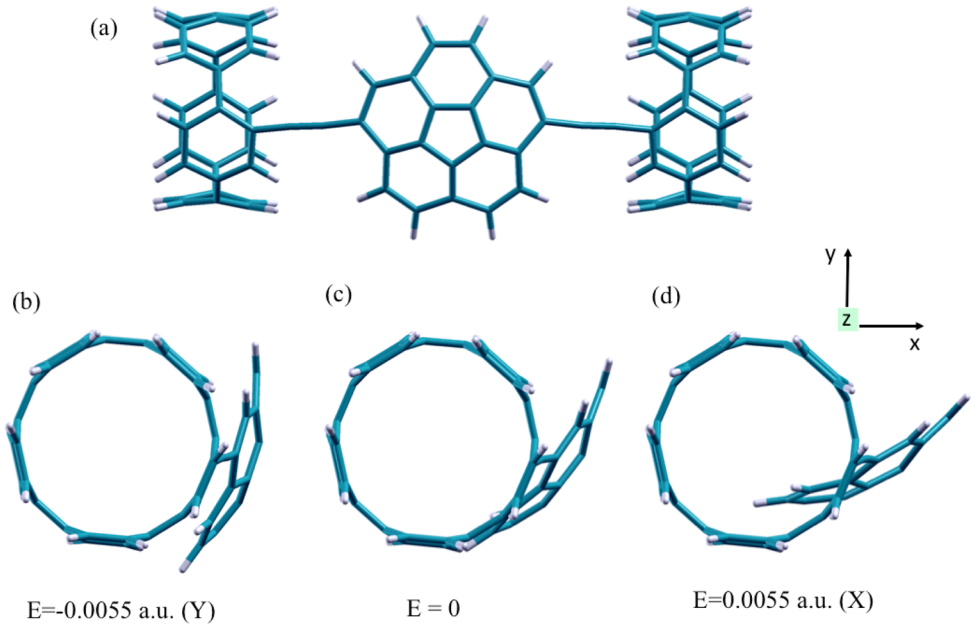

Figure 3. Molecular conformations of the "model junction" under the effect of an electric field.

$$\cos \vartheta_2 = \frac{P_0}{(\alpha_\perp - \alpha_\parallel)E_0} \quad (7)$$

The stability of this configuration depends on the sign of $\Delta\alpha = \alpha_\perp - \alpha_\parallel$. In fact, ϑ_2 is a minimum point when $\Delta\alpha > 0$ (i.e., the perpendicular polarizability is larger than that along the direction of the intrinsic dipole), and a maximum point otherwise. It is important to stress that, for all bowl-shaped aromatics considered, one finds $\Delta\alpha > 0$, which is thus the case of interest in this work.

A plot of total energy as a function of orientation angle for varying values of field strength as predicted by the analytical model is illustrated in Figure 2 for the smallest of the sequence of bowl-shaped aromatics, corannulene. The left panel corresponds to $\Delta\alpha > 0$, while the right panel corresponds to the $\Delta\alpha < 0$ case. Note that the case $\Delta\alpha < 0$ does not correspond to any of the physical systems investigated here but it is considered for the purpose of discussion.

DISCUSSION

It is important to take a deeper look into the physical interpretation of the results of the analytical model presented in the previous section. While for small fields the induced dipole is always smaller than the intrinsic dipole and the behavior of the system is governed by the intrinsic dipole in the field, when the field strength becomes large enough, the situation is different.

In the case of $\Delta\alpha < 0$, the polarizability along the direction of the intrinsic dipole is larger than the polarizability along the perpendicular direction. As a consequence, at low fields, the molecule preferentially orients its intrinsic dipole, P_0, along the electric field. When the field is strong enough, while the parallel orientation is still the minimum energy solution, a metastable local minimum is found for the molecule oriented antiparallel with respect to the electric field (here it is no longer the intrinsic dipole, but the induced dipole, that governs the orientation).

Even more interesting is the case when $\Delta\alpha > 0$, where the molecule is more polarizable in a direction orthogonal to the intrinsic molecular dipole. In this case, one expects to observe a crossover on the equilibrium position of the molecule, ranging from P_0 parallel to E at low fields, to the case where the induced perpendicular dipole dominates. This translates analytically into the stable position moving from ϑ_0 to ϑ_2 when the field is supercritical, progressing to $\pi/2$ where E_0 goes to infinity.

When $\Delta\alpha > 0$, validation of the analytical model is carried out by focusing on the case of corannulene and calculating the total energy (with respect to the zero field case) as a function of the angle between the field and the intrinsic molecular dipole for different field strengths (0.001 Ha a.u., 0.004 Ha a.u., 0.006 Ha a.u.). The computed values are shown as black points superimposed onto the continuous lines in Figure 2. This result shows the agreement between the analytic model and the calculated values to be excellent.

Considering the complete series $C_{20}H_{10}$−$C_{50}H_{10}$, the critical field defined in eq 6 can be evaluated for all fragments on the basis of the computed dipoles and polarizabilities. Using the plane-wave results of Tables 4 and 5, the following values of the critical field E_{crit} = 0.0045, 0.0073, 0.0149, and 0.0500 Ha a.u. (corresponding to 0.23, 0.38, 0.77, and 2.57 10^8 V/cm) are determined for the increasing curvature molecular bowls. Note that the value of the critical field tends to increase with the size of the molecule. This results from the increasing trend in intrinsic dipole P_0 with curvature in combination with the decreasing trend in $\Delta\alpha$ values, as discussed in the previous sections. Moreover, while these fields can be quite large for a molecular nanojunction,[33] reaching an overcritical situation can be considered realistic under such conditions, especially in the presence of field enhancement factors such as external tips or nanostructured electrodes.[33]

The behavior of the bowl fragments under an electric field becomes especially important when one would like to exploit the response to an electrical stimulus to govern the molecular orientation of the active element inside a molecular nanojunction. Such response opens the possibility to design and build efficient molecular switches. In fact, molecular switchability requires the existence of two isomers, which can be controllably converted from one to the other by some external stimulus. In this respect, a fundamental factor in the driving

force for switching is the ability to control the direction of the switching reaction so that the molecular conformation in the junction will show two extreme configurations with a significant on/off ratio. In this respect, it is worth noting that the predictions of the analytical model for the total energy of the system upon molecular orientation in the field (Figure 2) show that the energy gain due to molecular rotation can be quite consistent. For example, at a field of 0.006 Ha a.u., the molecule relaxes from an initial orientation having an angle ϑ of 180° to the field direction to a position where ϑ = 90°, with an energy gain of ∼0.25 eV.

Moving to larger molecules in the series, larger energy gains upon reorientation are expected, whether the field is under- or overcritical, because both P_0 and the polarizabilities increase with the size of the molecules. This suggests that molecular reorientation in a nanojunction due to the presence of an electric field can be feasible for all molecules in the series.

To corroborate the analytical model predictions with numerical calculations, a simplified example of a molecular junction is considered by focusing on the structural relaxation of a corannulene molecule linked to a (5,5) nanotube fragment (Figure 3), under the application of an electric field. The initial atomic coordinates have been extracted from a fully optimized calculation, including the seminfinite (5,5) nanotube and the corannulene molecular bowl, as described elsewhere.[34] In this prototypical junction, the initial molecular orientation corresponds to a ϑ angle between the intrinsic dipole and the electric field of about 180°, the only atoms free to relax being the ones of the molecular core, while the long arms of the molecule and the tube fragments are constrained in a fixed position.

From the initial configuration, the structure is relaxed without any electric field. Then structural relaxations under the following conditions are analyzed: (i) an electric field of 0.0055 Ha a.u. along the $+x$ direction (Figure 3d) and (ii) an electric field 0.0055 Ha a.u. along the $-y$ direction (Figure 3b). In both cases, the molecule is observed to rotate following the analytical model predictions. For instance, in the first case, the molecule was initially placed at ϑ = 180° and undergoes a rotation of ∼60° in the applied electric field.

To further investigate the interplay between the intrinsic and the induced dipoles, the model has also been applied to a noncurved π-conjugated molecule, specifically, the flat transition state structure of corannulene (Figure 4). The polarizabilities of the curved and flat conformation of corannulene are very similar ($\alpha_{\parallel}$ = 123 [Bohr^3], $\alpha_{\perp}$ = 307 [Bohr^3]; $\alpha_{\parallel}$ = 111 [Bohr^3], $\alpha_{\perp}$ = 320 [Bohr^3], respectively), but the analytical model prediction for the total energy gain upon molecular reorientation in the field is quite different for the two systems. In fact, while the induced dipoles can lead to a sensible energy gain from 180° to 90° degrees, the energy gain is considerably larger when the molecule possesses an intrinsic dipole. This confirms that the rotation of corannulene in the presence of an external field can be very effective if the field is placed properly (e.g., ϑ ∼180°), while this is not the case for the flat molecule.

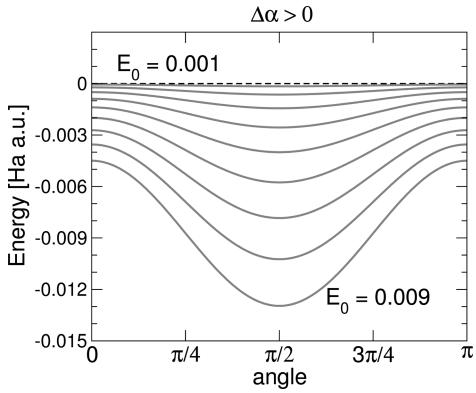

Figure 4. Model prediction for the total energy as a function of the molecule orientation with respect to external field for the case of planar $C_{20}H_{10}$: P_0 = 0.0 D, $\alpha_{\parallel}$ = 111 [Bohr^3], $\alpha_{\perp}$ =320 [Bohr^3]. Values for several field intensities are shown (ranging from 0.001 to 0.009 Ha a.u., with a step of 0.001 Ha a.u.).

CONCLUSIONS

In this work, the structural, electronic, and transport properties of a series of PAH systems of increasing curvature ($C_{20}H_{10}$−$C_{50}H_{10}$) are addressed by means of state-of-the-art theoretical techniques, enabling characterization of the electrical response properties of the systems. Semilocal (GGA-PBE, B97-D), meta-GGA (TPSS), and hybrid functionals (B3LYP, M06-2X) are considered and compared. Additionally, the plane-wave and pseudopotential methodology of Quantum-ESPRESSO using finite electric fields is compared to the all-electron localized basis description of GAMESS. On the basis of the results of first-principle approaches for electrical response functions of the bowl-shaped systems, an analytical model to describe the orientation of polarizable molecules under the influence of an external electric field is derived and validated for the case of a model molecular junction. The model is used to rationalize and predict the PAH fragment orientation under an electrical stimulus, suggesting the fundamental role of the intrinsic molecular dipole and linear polarizabilities in the resonse of the molecular systems. For shallow molecular bowls, dipoles induced across the relatively large surface area of the cap region may become comparable or larger than the intrinsic molecular dipole, thereby governing the molecular orientation in the field. On the other hand, for deeper bowls approaching a tube like structure, such an effect is not so apparent, since the magnitude of the polarizability along the molecular axis (z) aligns with the values along the x and y directions. From these results, it is clear that curvature and intrinsic molecular dipole are key factors in guiding molecular orientation in an external field and provide important design concepts for the construction of molecular switches based on curved aromatic bowl architectures.

AUTHOR INFORMATION

Corresponding Author

*Tel.: +41 44 635 4201. Fax: +41 44 635 6888. E-mail: kimb@oci.uzh.ch.

Notes

The authors declare no competing financial interest.

ACKNOWLEDGMENTS

We gratefully acknowledge the University of Zürich, UFSP program, and the Swiss National Science Foundation for support of this research. A.F. thanks Italian MIUR for partial support through Grant “EC SPECTRA” PRFR08F0AL 001.

REFERENCES

(1) Song, H.; Reed, M. A.; Lee, T. Single Molecule Electronic Devices. *Adv. Mater.* **2011**, *23*, 1583−1608.

(2) Borchardt, L.; Fuchicello, A.; Kilway, K. V.; Baldridge, K. K.; Siegel, J. S. Synthesis and Dynamics of the Corannulene Nucleus. *J. Am. Chem. Soc.* **1992**, *114*, 1921−1923.
(3) Filatov, A. S.; Scott, L. T.; Petrukhina, M. A. $\pi-\pi$ Interactions and Solid State Packing Trends of Polycyclic Aromatic Bowls in the Indenocorannulene Family: Predicting Potentially Useful Bulk Properties. *Cryst. Growth Des.* **2010**, *10*, 4607−4621.
(4) Sygula, A.; Saebo, S. $\pi-\pi$ Stacking of curved carbon networks: The corannulene dimer. *Int. J. Quantum Chem.* **2009**, *109*, 65−72.
(5) Peverati, R.; Baldridge, K. K. Implementation and optimization of DFT-D with respect to basis set and functional for Study of Dispersion Interactions in Nanoscale Aromatic Hydrocarbons. *J. Chem. Theory Comput.* **2008**, *4*, 2030−2048.
(6) Kennedy, M. R.; Burns, L. A.; Sherril, C. D. Buckyplates and Buckybowls: Examining the Effects of Curvature on $\pi-\pi$ Interactions. *J. Phys. Chem. A* **2012**, *116*, 11920−11926.
(7) Amaya, T.; Seki, S.; Moriuchi, T.; Nakamoto, K.; Nakata, T.; Sakane, H.; Saeki, A.; Tagawa, S.; Hirao, T. Anisotropic Electron Transport Properties in Sumanene Crystal. *J. Am. Chem. Soc.* **2009**, *131*, 408−409.
(8) Wu, Y.-T.; Bandera, D.; Maag, R.; Linden, A.; Baldridge, K. K.; Siegel, J. S. Multi-ethynyl Corannulenes: Synthesis, Structure and Properties. *J. Am. Chem. Soc.* **2008**, *130*, 10729−10739.
(9) Zoppi, L.; Martin-Samos, L.; Baldridge, K. K. Effect of Molecular Packing on Corannulene-Based Materials Electroluminescence. *J. Am. Chem. Soc.* **2011**, *133*, 14002−14009.
(10) Lovas, F. J.; McMahon, R. J.; Grabow, J.-U.; Schnell, M.; Mack, J.; Scott, L. T.; Kuczkowski, R. L. Interstellar Chemistry: A Strategy for Detecting Polycyclic Aromatic Hydrocarbons in Space. *J. Am. Chem. Soc.* **2005**, *127*, 4345−4349.
(11) Molen, S. J. v. d.; Liljeroth, P. Charge transport through molecular switches. *J. Phys.: Condens. Matter* **2010**, *22*, 133001−1−30.
(12) Hohenberg, P.; Kohn, W. Inhomogeneous Electron Gas. *Phys. Rev.* **1964**, *136*, B864−B871.
(13) http://www.msg.ameslab.gov/gamess/ (accessed date August 2013).
(14) Frisch, M. J.; Trucks, G. W.; Schlegel, H. B.; Scuseria, G. E.; Robb, M. A.; Cheeseman, J. R.; Scalmani, G.; Barone, V.; Mennucci, B.; Petersson, G. A.; Nakatsuji, H.; Caricato, M.; Li, X.; Hratchian, H. P.; Izmaylov, A. F.; Bloino, J.; Zheng, G.; Sonnenberg, J. L.; Hada, M.; Ehara, M.; Toyota, K.; Fukuda, R.; Hasegawa, J.; Ishida, M.; Nakajima, T.; Honda, Y.; Kitao, O.; Nakai, H.; Vreven, T.; Montgomery, J. A., Jr.; Peralta, J. E.; Ogliaro, F.; Bearpark, M.; Heyd, J. J.; Brothers, E.; Kudin, K. N.; Staroverov, V. N.; Kobayashi, R.; Normand, J.; Raghavachari, K.; Rendell, A.; Burant, J. C.; Iyengar, S. S.; Tomasi, J.; Cossi, M.; Rega, N.; Millam, N. J.; Klene, M.; Knox, J. E.; Cross, J. B.; Bakken, V.; Adamo, C.; Jaramillo, J.; Gomperts, R.; Stratmann, R. E.; Yazyev, O.; Austin, A. J.; Cammi, R.; Pomelli, C.; Ochterski, J. W.; Martin, R. L.; Morokuma, K.; Zakrzewski, V. G.; Voth, G. A.; Salvador, P.; Dannenberg, J. J.; Dapprich, S.; Daniels, A. D.; Farkas, Ö.; Foresman, J. B.; Ortiz, J. V.; Cioslowski, J.; Fox, D. J. *Gaussian 09*; Gaussian, Inc.: Wallingford, CT, 2009.
(15) Perdew, J. P.; Burke, K.; Ernzerhof, M. Generalized Gradient Approximation Made Simple. *Phys. Rev. Lett.* **1996**, *77*, 3865−3868.
(16) Zhao, Y.; Schultz, N. E.; Truhlar, D. G. Exchange-correlation functional with broad accuracy for metallic and nonmetallic compounds, kinetics, and noncovalent interactions. *J. Chem. Phys.* **2005**, *123*, 1−4.
(17) Hertwig, R. H.; Koch, W. On the parameterization of the local correlation functional: What is Becke-3-LYP? *Chem. Phys. Lett.* **1997**, *268*, 345−351.
(18) Stephens, P. J. D.; Chabalowski, C. F.; Frisch, M. J. Ab Initio Calculation of Vibrational Absorption and Circular Dichroism Spectra Using Density Functional Force Fields. *J. Phys. Chem.* **1994**, *98*, 11623−11627.
(19) Zhao, Y.; Truhlar, D. G. The M06 Suite of Density Functionals for Main Group Thermochemistry, Thermochemical Kinetics, Noncovalent interactions, Excited States, and Transition Elements: Two New Functionals and Systematic Testing of Four M06 Functionals and Twelve Other Functionals. *Theor. Chem. Acc.* **2008**, *120*, 215−241.
(20) Tao, J.; Perdew, J. P.; Staroverov, V. N.; Scuseria, G. E. Climbing the Density Functional Ladder: Nonempirical Meta−Generalized Gradient Approximation Designed for Molecules and Solids. *Phys. Rev. Lett.* **2003**, *91*, 146401−1−4.
(21) Perdew, J. P.; Tao, J.; Staroverov, V. N.; Scuseria, G. E. Meta-generalized gradient approximation: Explanation of a realistic nonempirical density functional. *J. Chem. Phys.* **2004**, *120*, 6898−6911.
(22) Grimme, S. J. Semiempirical GGA-type density functional constructed with a long-range dispersion correction. *J. Comput. Chem.* **2006**, *27*, 1787−1799.
(23) Chai, J.-D.; Head-Gordon, M. Systematic optimization of long-range corrected hybrid density functionals. *J. Chem. Phys.* **2008**, *128*, 084106−1−14.
(24) Dunning, T. H. J. Gaussian Basis Sets for Use in Correlated Molecular Calculations. I. The Atoms Boron Through Neon and Hydrogen. *J. Chem. Phys.* **1989**, *90*, 1007−1023.
(25) Weigend, F.; Ahlrichs, R. Balanced basis sets of split valence, triple zeta valence and quadruple zeta valence quality for H to Rn: Design and assessment of accuracy. *Phys. Chem. Chem. Phys.* **2005**, *7*, 3297−3305.
(26) Rappoport, D.; Furche, F. Property-optimized Gaussian basis sets for molecular response calculations. *J. Chem. Phys.* **2010**, *133*, 134105-1−11.
(27) Baldridge, K. K.; Greenberg, J. P. QMView: A Computational 3-D Visualization Tool at the Interface Between Molecules and Man. *J. Mol. Graphics* **1995**, *13*, 63−66.
(28) http://www.webmo.net/index.html (accessed date August 2013).
(29) http://qe-forge.org/gf/project/q-e/ (accessed date August 2013).
(30) Martyna, G. J.; Tuckerman, M. E. A reciprocal space based method for treating long range interactions in ab initio and force-field-based calculations in clusters. *J. Chem. Phys.* **1999**, *110*, 2810−2821.
(31) Seiders, T. J.; Baldridge, K. K.; Grube, G. H.; Siegel, J. S. Structure/Energy Correlation of Bowl Depth and Inversion Barrier in Corannulene Derivatives: Combined Experimental, and Quantum Mechanical Analysis. *J. Am. Chem. Soc.* **2001**, *123*, 517−525.
(32) Haddon, R. C.; Scott, L. T. π-Orbital conjugation and rehybridization in bridged annulenes and deformed molecules in general: π-orbital axis vector analysis. *Pure Appl. Chem.* **1986**, *58*, 137−142.
(33) Rahimi, M.; Troisi, A. Probing local electric field and conformational switching in single-molecule break junctions. *Phys. Rev. B* **2009**, *79*, 113413−1−4.
(34) Zoppi, L.; Ferretti, A.; Baldridge, K. K. Manuscript in preparation.